State-selective electron capture by 18-keV Kr^{8+} ions from laser-excited $Rb^*(15p-25p)$ Rydberg atoms

A. Pesnelle,[1] J. Pascale,[1] R. Trainham,[1,*] and H. J. Andrä[2]
[1]*Service des Photons, Atomes et Molécules, DRECAM, CEA/Saclay, 91191 Gif-sur-Yvette-Cedex, France*
[2]*Institut für Kernphysik, Universität Münster, Wilhelm Klemm Strasse 9, 48149 Münster, Germany*
(Received 18 April 1996)

State-selective single electron capture, in collisions of multicharged ions Kr^{8+} at 18 keV with laser-excited Rydberg $Rb^*(n_ip)$ atoms, is investigated by use of a field ionizing lens system (FILS), in a three-crossed-beam experiment. By scanning the laser over a wide range of wavelengths (303–298 nm), this investigation covers the $15p-25p$ Rydberg series, showing the influence of the initial state of Rb. For every well-defined $Rb^*(n_ip)$ state, (i) very high Rydberg states of the $Kr^{7+*}(n)$ product ions are detected as a consequence of the high degree of excitation of the target and of the high charge of the projectile, and (ii) the n distribution of the capture cross section is obtained in the domain $67 \leqslant n \leqslant 95$, by measuring the energy spectrum of the Kr^{8+} ions produced by field ionization in the FILS of the excited product ions Kr^{7+*}. These n distributions become wider and are systematically shifted towards higher n values as n_i increases. By using the classical trajectory Monte Carlo method, the n distributions are calculated for the n_ip series. Although the calculated n distributions are systematically wider, the behavior of their widths and of their relative positions is in agreement with the experiment. On the other hand, the extended classical over-the-barrier model yields n distributions significantly narrower than the experimental ones. [S1050-2947(96)00811-6]

PACS number(s): 34.70.+e, 34.60.+z, 34.50.Rk

I. INTRODUCTION

Single electron capture from an atomic ground state into a multicharged ion A^{q+} takes place into relatively low n orbitals of the product ion $A^{(q-1)+}(n)$, even in the case of alkali-metal atoms for which the binding energy of the valence electron is small. Within the classical model [1–3], orbitals with n close to 10 are mainly populated for $q=8$ and Rb target atoms. Large capture cross sections due to the high charge of the projectile are expected, increasing almost proportionally to q, for q larger than some units.

These large capture cross sections are limited, however, to a domain of impact velocities below and around the matching velocity $\tilde{v}=1$, where $\tilde{v}$, the so-called reduced velocity, is defined by v_p/v_e, the ratio of the multicharged projectile velocity v_p and the orbital electron velocity v_e in the target atom. In the practical example of Kr^{8+} on Rb(5s), a classical cross section of order of magnitude equal to 10^{-13} cm^2 is obtained for a kinetic energy close to 80 keV/charge (i.e., $\tilde{v}=1$).

Using the scaling laws of the classical model, it is also seen that the total single electron capture cross section σ_t is inversely proportional to the square of the electron binding energy in the target atom $\epsilon_{\rm at}$. Atoms with a very weakly bound electron would therefore be exceptional targets for strongly enhanced capture processes: a reduction of the binding energy by a factor of 100 means an increase by a factor of 10^4 of the cross section which approaches 10^{-9} cm^2, i.e., the micrometric range (0.1 μm^2).

Simultaneously, because of the quasiresonance of the charge-transfer process, orbitals much higher than $n \simeq 10$ would be populated. Classical scaling laws show that the ratio n/n_i increases with q as $q^{0.81}$ within 3%, where n and n_i are the principal quantum numbers of the captured electron in the final product ion and in the initial target atom, respectively.

Laser excitation combined with a field-ionizing lens system (FILS) has made it possible to detect very high $Kr^{7+*}(n)$ Rydberg states after single electron capture from $Rb^*(17p)$ atoms into Kr^{8+} multicharged ions, and to measure the n distribution of final states [4], for the two collision energies 18 and 40 keV.

There is a great lack of experimental work relevant to this type of multicharged ion plus Rydberg-atom collision. To date, final-state distributions after charge transfer from Rydberg atoms were observed via field ionization by MacAdam and co-workers for singly charged projectiles, such as Ar^+ and Na^+ ions, over the energy range 60–2100 eV. This corresponds to a reduced velocity $\tilde{v} \simeq 0.2$–2.0, when bombarding laser-excited $Na^*(n_il_i)$ atoms in $n_il_i = 24d$, $28d$, and $33d$, and $25s$, $29s$, and $34s$ states [5–7]. The observed n distributions of the $Ar^*(n)$ and $Na^*(n)$ reaction products, which are neutrals in this case, extend typically from $n \simeq 20$ to $n \simeq 50$. The replacement of singly charged projectiles by multicharged ions in collisions with Rydberg atoms pushes the final-state orbitals to still higher n values, as observed up to 110 in Ref. [4]. However, compared to field ionization of neutrals, field ionization of fast highly excited multiply charged ions such as Kr^{7+*} is complicated by the sensitivity of the trajectories to any field, including the ionizing field itself; this is the primary experimental difference between the present experiment and that of MacAdam and co-workers.

At the beginning of this field of collisions of multicharged ions with laser-excited atoms, the resonant state $Na^*(3p)$

*Present address: STID, DRFC, CEA/Cadarache, 13108 St. Paul-lez-Durance-Cedex, France.

obtained by laser excitation at the easily produced wavelength of 589 nm was mainly used as a target. An experiment was performed by Aumayr and co-workers with He^{2+} projectiles, where translational energy spectroscopy of the product ions $He^{+}*(n)$ was used to study state-selective capture [8] and alignment effects on the capture cross section [9,10]. The combination of a small projectile charge ($q=2$) and a still rather high binding energy (for the resonant target electron $\epsilon_{at}=2.10$ eV) ends up in captures in relatively low excited states $n=3$, 4, and 5 of the product ion. The same kind of alignment experiment with $Na*(3p)$ target atoms has been developed as a function of the collision energy by using the detection of the fluorescence photons emitted by the product ions. Schlatmann and co-workers used He^{2+} projectiles and observed the $He^{+}*(4l\rightarrow 3l')$ transitions [11], and Schippers and co-workers used the more highly charged projectiles O^{6+} leading to higher excited levels $n=6$–15 among which the $O^{5+}*(10l\rightarrow 8l')$ transitions were detected [12].

Recently, DePaola and co-workers obtained absolute values of total (without state selection) electron capture cross sections for Xe^{q+} ($q=8,16,32,40$) projectiles colliding with $Rb*(10f)$ [13]. For this purpose, the target atoms were excited via the $5s\rightarrow 5p\rightarrow 4d\rightarrow 10f$ steps by superposition of three laser beams, and the total diminution of the primary Xe^{q+} beam was measured when the laser excitation was turned on. The very high cross sections predicted by the classical model are actually obtained: they show a maximum of some 10^{-10} cm^2 for $\tilde{v}=1$ and a fast decrease when $\tilde{v}$ increases to 3.

In this paper we describe the experimental procedure of our investigation in more detail than in our Letter [4], and report on the extension of our measurements to a series of $n_i p$ Rydberg states of the Rb target atom. All the states from $n_i=15$ to $n_i=25$ were investigated by scanning the uv laser over a wide domain of wavelengths (from 303.29 to 298.76 nm), and by measuring the n distribution of the capture cross section for every Rydberg state in order to show the influence of the initial state of Rb.

Such high $Kr^{7+}*$ Rydberg ions are semiclassical in nature; therefore the electron capture should be well described by a classical model. In particular, the three-body classical trajectory Monte Carlo (CTMC) method, as successfully used in previous studies of ion and Rydberg-atom collisions [14,15], is well suited to treat these collisions, implying high excited states in both the target atom and the product ion. For these collisions, conventional quantum mechanical methods are inapplicable in view of the large number of molecular or atomic basis states to consider in the close-coupling calculations, which must include both excitation and ionization channels. Those are implicitly included in the CTMC method. Details on these calculations, which use model potentials to describe the interaction between the excited electron in $Rb*(n_i p)$ and the ionic Rb^+ and Kr^{8+} cores [15,16], are given in Sec. IV.

II. EXPERIMENT

A. Experimental setup

The state-selective electron capture from laser-excited $Rb*(n_i p)$ atoms into multicharged Kr^{8+} ions is carried out in a three-crossed-beam apparatus, using a field ionization technique (see Fig. 1).

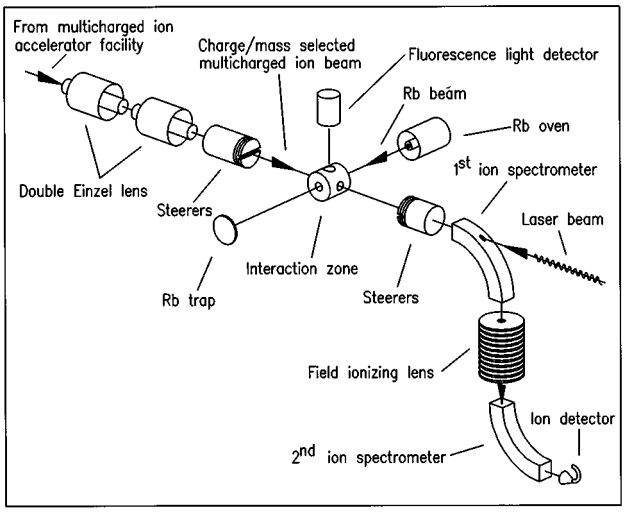

FIG. 1. Schematic diagram of the apparatus. Only the terminal part including the interaction and the detection chambers is shown.

1. The multicharged ion beam

The Kr^{8+} ion beam is delivered by the accelerator of multicharged ions (AIM) in Grenoble, where the beam-transport optics have been especially designed and built to provide a high quality emittance $e \leqslant 45\pi$ mm×mrad, and a beam of high brilliance by Andrä and co-workers [17].

In order to reduce the degradation of the emittance by Coulomb explosion of the mA's of the extracted beam, the highest extraction voltage from the electron cyclotron resonance Caprice ion source is used, and the separation of all unwanted q/m takes place as close as possible to the extraction region. To this end, the source is put on the user-defined low positive potential V_s and the charge and mass separation is effected by a double focusing magnet with its vacuum chamber at a negative voltage V_{mag}, summing up to a total extraction voltage of usually $V_s + |V_{mag}| = 20$ kV. After q/m separation, the selected ions are decelerated by climbing from the negative potential V_{mag} to ground. This deceleration is controlled by a double Einzel lens which also focuses the beam into a first diagnostic chamber. With $V_s = 2.25$ kV and $V_{mag} = -17.75$ kV, a low-energy beam with 2.25 kV/q, i.e., a Kr^{8+} beam with a total kinetic energy $E_0=18$ keV, is obtained in the present experiment. With $V_s=5$ kV and $V_{mag}=-15$ kV, a beam with 5 kV/q, i.e., a Kr^{8+} beam with a higher kinetic energy $E_0=40$ keV, is obtained as in our Letter [4]. For both energies, an energy spread of the multicharged ion beam ΔE_0 smaller than 20 eV can be deduced from the performances of the accelerator, as verified in numerous experiments, which corresponds to a relative energy spread $\Delta E_0/E_0$ smaller than 1.1×10^{-3} at 18 keV, and 5×10^{-4} at 40 keV, respectively.

After passing through a second double focusing magnet, the ion beam is vertically and horizontally shaped by an electric quadrupole triplet. Then, it is guided towards the experiment via a switching magnet with a focal point in its center, and focused by an Einzel lens in a second diagnostic chamber which contains horizontal and vertical steerers, a set of circular apertures, and a movable Faraday cup (FC1).

A double Einzel lens with a variable magnification, in a differentially pumped vacuum chamber, serves to focus the beam from the center of the second diagnostic chamber to

the point of interaction with the Rb beam. This point is located inside the interaction vacuum chamber which contains also two sets of vertical and horizontal steerers and two 2-mm-diam diaphragms in symmetrical positions with respect to the interaction point. They are used for optimization of intensity and quality (in shape) of the primary Kr^{8+} and product $Kr^{7+}*$ ion beams.

Typical intensities on the FC1 of Kr^{8+} ions are 2.7 μA for $E_0=40$ keV and 0.8 μA for $E_0=18$ keV.

2. Laser excitation of $Rb^*(n_ip)$ atoms

The excitation of a single Rydberg level of Rb from the ground state requires narrow bandwidth uv radiation at 300 nm: from 303.29 nm for the 15p level to 298.76 nm for the 25p level. It is generated by intracavity frequency doubling [i.e., second harmonic generation (SHG)] in a single-mode cw ring dye laser (Spectra-Physics 380D), frequency stabilized with the reference interferometer system (Spectra-Physics 488), as in our numerous experiments on He Rydberg atoms [18]. The laser is operated with Rhodamine-6G and with a 2.3-cm-long AD*A crystal (ammonium dihydrogen arsenate) in noncritical 90° phase matching. With about 4.5 W of Ar^+ pump laser power at 514.5 nm (Coherent Innova100), we obtained about 6 to 7 mW of single-mode, continuously tunable, cw, uv radiation at 300 nm with a full width at half maximum (FWHM) of 2 MHz. Our procedure for SHG has been described in detail by Runge and coworkers [19].

The tuning range of the laser is large enough to directly excite the one-photon $5s\rightarrow n_ip$ Rydberg transitions up to the ionization limit. Optimization of the uv power is achieved by readjusting the crystal temperature at resonance. This technique, which deals with only one photon, offers a great advantage over the stepwise excitation technique where the superposition of several (often three) laser beams in the interaction zone is necessary to reach Rydberg states. Furthermore, the present procedure is cw with the best possible duty cycle.

Calculations of Rydberg-state lifetimes provide orders of magnitude of 5 μs for the 15p level to 32 μs for the 25p level [20]. Consequently, Rb* atoms with a mean velocity of 380 m/s cover a mean distance of 2 to 12 mm which is longer than the laser spot in the interaction region. Loss of excited states by an optical-pumping process towards the hyperfine ground-state levels is therefore expected to be negligible.

The detection of the optical resonances occurring from the 5s ground state for ^{85}Rb($F=2,3$) and ^{87}Rb($F=1,2$) to the n_ip Rydberg levels is effected by measuring the fluorescence photons of the strongest cascades in the visible far red, such as $n_ip\rightarrow 4d$ (708–743 nm), together with the resonance line $5p\rightarrow 5s$ (780 and 795 nm), by a photomultiplier with a color filter. The hyperfine structure (hfs) spectrum of the transition $5s\ ^2S_{1/2}\rightarrow 20p\ ^2P_{3/2}$ for ^{85}Rb and ^{87}Rb has been recorded by scanning the laser continuously over a 10-GHz range. It exhibits the clearly resolved and expected four lines of the ground-state splitting since the hyperfine levels of the high Rydberg states are nearly degenerate [21]. The strongest hyperfine component of the ^{85}Rb line, i.e., $5s\ ^2S_{1/2}(F=3)\rightarrow n_ip\ ^2P_{3/2}$, is used for the experiment of electron capture, and the fluorescence photons are used to monitor the excited atom density during the $Kr^{7+}*$ ion detection. A stable uv beam is achieved over several hours with the laser locked on the chosen transition via the reference interferometer system, since the residual broadening of 400 MHz (FWHM) due to the uncollimated Rb beam is sufficiently wide.

3. The interaction region

In the interaction region, the Kr^{8+} beam perpendicularly intersects the Rb beam effusing from a resistance heated oven (typical temperature from 450 to 525 K) via its 1-mm-diam $\times$ 2-mm-long exit pipe which is overheated to 570 K to suppress dimers. The uv beam is sent into the interaction region anticollinearly with respect to the ion beam; the Rb atoms are therefore illuminated over the complete width of the Rb beam.

The interaction region is located inside a small copper box which can be biased electrically, if necessary, to a potential V_t in order to modify the collision energy. The potential V_t is also used to separate the two kinds of $Kr^{7+}*$ ions: those due to electronic capture on Rb atoms inside the copper box, which leave it with an energy E_0-qeV_t, and those due to electronic capture on background gas atoms elsewhere along the Kr^{8+} beam, which leave the copper box with an energy E_0. It has been verified that this second contribution is negligible, and consequently V_t could be grounded in most of the experiments.

Baking the experimental setup yields a background pressure in the interaction chamber of some 10^{-10} mb with the Rb beam off, and about 10^{-7} mb after a one-day run of about 15 h with the Rb beam on.

4. The field ionization detector

After electron capture, the $Kr^{7+}*$ ions leave the interaction zone and pass through the downstream steerers and diaphragm. They then enter the detection vacuum chamber where a high vacuum is maintained ($\simeq 10^{-9}$ mb with the Rb beam on). The $Kr^{7+}*$ ions are then separated from the rest of the ion beam, which is mainly composed of Kr^{8+} projectiles, by a first electrostatic spectrometer (SP1) which focuses the $Kr^{7+}*$ beam from the interaction zone to the entrance of the FILS.

The FILS is a cylindrically symmetric electrostatic field ionization lens, especially designed for the present experiment [22]. Compared to field ionization of neutrals, field ionization of highly excited multiply charged ions such as $Kr^{7+}*$ is complicated by the sensitivity of the trajectories to any field, including the ionizing field itself. This is the reason we have adopted a geometry where the electric field is collinear to the $Kr^{7+}*$ ion beam. The FILS is composed of 11 circular electrodes at suitable electrical potentials, equally spaced over a total length of 100 mm, with a circular hole in their center, sufficiently large to avoid strong focusing effects.

Symmetric voltages about the center z_c of the FILS prevent the kinetic energy of an ion at the lens entrance from being modified when it leaves the FILS without being field ionized. It creates on its z axis a negative $U(z)$ potential, quadratically decreasing from 0 at the lens entrance towards its center z_c where it reaches its minimum (its maximum in

absolute value). $U(z)$ then quadratically increases from z_c towards the lens exit where it reaches again 0.

Consequently, the FILS generates an electric field $F(z)$, linearly increasing from 0 at the lens entrance to its maximum F_m which is reached about 10 mm in front of z_c. The field decreases rapidly from F_m to 0 at z_c where it is inverted; then it decreases rapidly to $-F_m$, and linearly reincreases to 0 at the lens exit. Two sets of potentials have been applied on the 11 electrodes. The first one requires -20 kV on the center electrode; it is composed of the voltages 0.0, -0.8, -3.2, -7.2, -12.8, -20.0, -12.8, -7.2, -3.2, -0.8, and 0.0 kV which generate the maximum field F_m = 5.2 kV/cm. The second set requires -35 kV on the center electrode; it is composed of the voltages 0.0, -1.4, -5.6, -12.6, -22.4, -35.0, -22.4, -12.6, -5.6, -1.4, and 0.0 kV which generate the maximum field F_m = 9.1 kV/cm. The latter has been used in the measurements presented in this paper.

When a $Kr^{7+}*$ ion in a Rydberg state n_j enters the FILS, it experiences an electric field with increasing strength in the first half of the FILS. It is field ionized and becomes a Kr^{8+} ion at the critical field F_j at the distance z_j, with the corresponding potential U_j. During the first half of the FILS, it is accelerated as a seven-times charged particle until z_j, then as an eight-times charged particle until z_c. In the second half of the FILS, it is then decelerated as an eight-times charged particle. It is therefore more decelerated than accelerated, and the resulting Kr^{8+} ion has lost an amount of kinetic energy equal to $e|U_j|$ when leaving the FILS.

These Kr^{8+} ions are then analyzed as a function of their kinetic energy and separated from the rest of the ion beam by a second electrostatic spectrometer (SP2) which focuses the ion beam from the exit diaphragm of the FILS to the detector. The detector is either a Faraday cup (FC2) for measuring the projectile beam, or an electron multiplier (EM) for counting the Kr^{8+} ions after field ionization of the $Kr^{7+}*$ product ions. The two spectrometers SP1 and SP2 are identical; they are 100-mm midradius spherical analyzers, with two 90° sectors closely spaced (15 mm), which double focus the ion beam in both the deflection plane and the perpendicular plane. In order to achieve a high-energy resolution of the whole system, two 1.5-mm-diam diaphragms were introduced at the entrance and exit electrodes of the FILS, one 2-mm-diam and one 1.5-mm-diam diaphragm downstream the SP2 exit before entering the cone of the electron multiplier.

The FILS has been conceived to yield a constant transmission for all the ion trajectories, especially when charge-changing ionization takes place somewhere inside the FILS. A Monte Carlo simulation of the $Kr^{7+}*$ and Kr^{8+} ion trajectories through the FILS, and through the whole detection system composed of the FILS plus the spectrometer SP2 plus the downstream diaphragms has been performed. It includes Kr^{8+} projectile trajectories, $Kr^{7+}*$ product-ion trajectories, and $Kr^{7+}*$,Kr^{8+} product-ion trajectories with $Kr^{7+}* \rightarrow Kr^{8+}$ charge changing when field ionization occurs at different positions along the trajectories in the FILS. The usual experimental beam conditions are defined by $E_0 = 18$ keV, the electrodes biased according to the second set of potential values, and a half angle of beam opening of 10 mrad ($\simeq 0.6°$). The transmission of the FILS is then 1.0 for any position of field ionization of $Kr^{7+}*$ in the FILS; the transmission of the whole detection system is 0.58 with a standard deviation of 0.05 [23]. This result demonstrates that the detection system does not introduce substantial discrimination among the various trajectories without or with field ionization whatever the position of charge changing is inside the FILS.

B. Experimental procedure

In the interaction zone, the kinetic energy of the Kr^{q+} projectile ions is

$$E_t = E_0 - qeV_t, \tag{1}$$

where $q = 8$ in the present work.

The $Kr^{(q-1)+}*$ ions are produced by electronic capture with a kinetic energy $E_t' = E_t + Q$, where Q is the so-called energy gain (positive or negative), defined via the conservation of the total energy of the colliding system by $Q = \epsilon_{\text{ion}} - \epsilon_{\text{at}}$ [3]. In the present study, with Rydberg states in both the initial and final channels, the binding energies are small: ϵ_{at} varies from 0.089 to 0.027 eV over the $Rb*(n_i p)$ Rydberg series with $n_i = 15$ to 25; ϵ_{ion} varies from 0.194 to 0.096 eV over the $n = 67-95$ range of detected $Kr^{7+}*(n)$ final states. Consequently, $Q(n_i, n)$ varies over a range of very small values, from 0.007 to 0.17 eV (corresponding to 1×10^{-4} to 3×10^{-3} V for the spectrometer voltage V_{sp}). $Q(n_i, n)$ is therefore neglected in the data analysis (this omission has been verified to have no consequence on the cross sections experimentally obtained), and the $Kr^{(q-1)+}*$ ions can be considered as produced with the same kinetic energy as the Kr^{q+} projectiles. In the interaction zone, the kinetic energy of the $Kr^{(q-1)+}*$ ions produced by capture from $Rb*$ atoms is

$$E_t' = E_t. \tag{2}$$

At the SP1 entrance, the kinetic energy of Kr^{q+} projectiles is E_0 whatever V_t is, since the potential on the midradius of the spectrometer is zero and a reacceleration equivalent to the deceleration before the interaction zone takes place after the interaction zone (between the interaction box and the SP1). The kinetic energy of the $Kr^{(q-1)+}*$ product ions is, however, modified since they are less reaccelerated due to their $(q-1)$ charge. It is equal to $E_0' = E_t' + (q-1)eV_t$, which becomes

$$E_0' = E_0 - eV_t, \tag{3}$$

according to Eqs. (1) and (2).

After passing through the FILS, the Kr^{q+} projectiles keep their kinetic energy, while that of the $Kr^{(q-1)+}*$ in a state n_j is modified according to the distance z_j of charge changing: the final kinetic energy of the resulting Kr^{q+} ions is $E_f' = E_0' + eU_j$ where U_j is always negative, i.e.,

$$E_f' = E_0 - eV_t - e|U_j|. \tag{4}$$

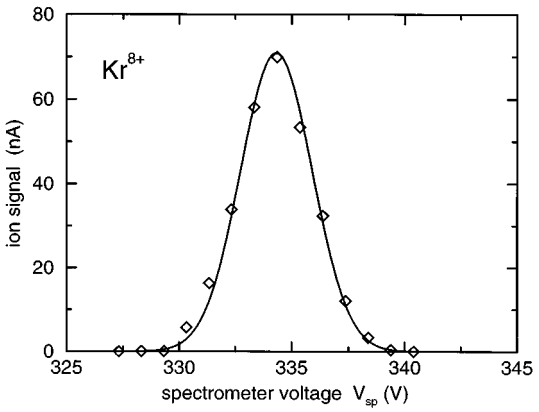

FIG. 2. Kr^{8+} projectile-ion spectrum measured on a movable Faraday cup which replaces the channeltron shown in Fig. 1, as a function of the SP2 spectrometer voltage V_{sp} (in V): $\diamond$, experimental points; continuous line, Gaussian fit. Since the kinetic energy of the multicharged ion beam is sharply defined (see Sec. II A 1), this curve represents the transmission function of the detection system. The Kr^{8+} kinetic energy is related to the SP2 spectrometer voltage by $\simeq 54.4\times V_{sp}$ (in eV), corresponding to $k\simeq 0.147$ (with $q=8$).

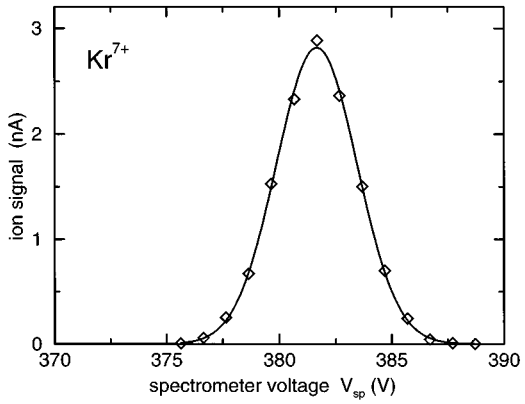

FIG. 3. Capture from Rb($5s$) into Kr^{8+}: Kr^{7+} product-ion spectrum (as in Fig. 2). Since the kinetic energy of the multicharged ion beam is sharply defined (see Sec. II A 1) and the energy gain is negligible (see Sec. II B), this curve represents the transmission function of the detection system. The Kr^{7+} kinetic energy is related to the SP2 spectrometer voltage by $\simeq 47.6\times V_{sp}$ (in eV), corresponding to $k\simeq 0.147$ (with $q=7$).

In the present experiment, the low value of the kinetic energy $E_0=18$ keV has been obtained directly by adjusting V_s. The interaction box has been kept grounded, i.e., $V_t=0$, except for a test of verification that no substantial capture takes place on the background gas along the path of the projectile beam outside of the interaction zone. Consequently, the energy analysis in the SP2 is made on the basis of

$$E_f'=E_0-e|U_j|. \tag{5}$$

The first step of the experimental procedure consists in measuring, after optimization, the Kr^{8+} projectile ion signal on the Faraday cup FC2, with the SP1 and SP2 both tuned to the charge $q=8$ for the energy $E_0=18$ keV. The high voltages are already applied on the FILS in order to optimize the ion trajectories for the final experimental conditions. Scanning the SP2 symmetric voltages yields the corresponding ion spectrum shown in Fig. 2; a typical Gaussian curve centered at 334.3 V is obtained.

In a second step, the $Kr^{7+}*(n)$ ion signal is measured on the FC2; it is formed by electronic capture on ground-state Rb($5s$) atoms in the interaction box. This process mainly populates the orbital $n=10$ which is not field ionized in the FILS. For this measurement, the SP1 and SP2 are both tuned to the charge $(q-1)=7$ for the energy $E_0'\simeq E_0=18$ keV [the energy gain $Q(5s,10)$ is about 4 eV, corresponding to 0.08 V for the spectrometer voltage V_{sp}: it can be neglected]. Scanning the SP2 symmetric voltages yields the corresponding ion spectrum shown in Fig. 3: a typical Gaussian curve centered at 381.7 V is obtained.

From these measurements, one can confirm the value of the calibration parameter k for the SP2 which is the ratio of the spectrometer voltage V_{sp} (in V) applied to both sectors (one sector with $+V_{sp}$, the other with $-V_{sp}$) and the ion kinetic energy per charge E_0/q (in eV/charge). When taking into account the positive plasma potential inside the ion source and the calibration of the V_s potential, E_0 is found to be 18.17 keV. One finds, therefore, $k\simeq 0.147$. Since the kinetic energy of the multicharged ion beam is sharply defined, $\Delta E_0<20$ eV (FWHM) (see Sec. II A 1) corresponding to $\Delta V_{sp}<0.37$ V, the Gaussian curves shown in Figs. 2 and 3 represent the transmission function of the experimental detection system. The average value of the detection system resolution is deduced from these spectra: one finds $R\simeq 90$ (FWHM) [i.e., $\Delta E_f'/E_f'=\Delta V_{sp}/V_{sp}=1.1\%$ (FWHM)].

The third step of the experimental procedure consists in measuring the high Rydberg $Kr^{7+}*(n)$ ion signal on the channeltron EM stemming from electronic capture on laser-excited Rb* atoms in the interaction zone. This process populates very high n orbitals which are field ionized in the FILS. To this end, the SP1 is tuned to the charge $(q-1)=7$ for the energy $E_0'=E_0=18$ keV, and the SP2 tuned to the charge $q=8$ for an energy E_f' given by Eq. (5). The energy distribution of these Kr^{8+} ions is measured with the SP2 by scanning its voltage. The abundance of Kr^{8+} ions at the energy E_f' corresponds to that of $Kr^{7+}*$ ions with a Rydberg electron in level n_j.

We observe that the signal of capture on laser-excited Rb* atoms is much smaller than that on Rb($5s$) atoms, in spite of much larger cross sections. This is the consequence of a very small ratio $\rho^*\delta l^*/\rho\delta l$, where ρ^* and ρ, δl^* and δl are the density and the thickness of the Rb* and Rb ($5s$) atomic target, respectively. This is mainly due to the low effective laser intensity inside the collision chamber; it will be seen in Sec. III, however, that the high sensitivity and selectivity of the detection method overcome the small excitation rate.

III. EXPERIMENTAL RESULTS

A. Ion energy spectra

The procedure described in Sec. II B is repeated for every excited n_ip state of Rb. Of the whole series $15\leqslant n_i\leqslant 25$,

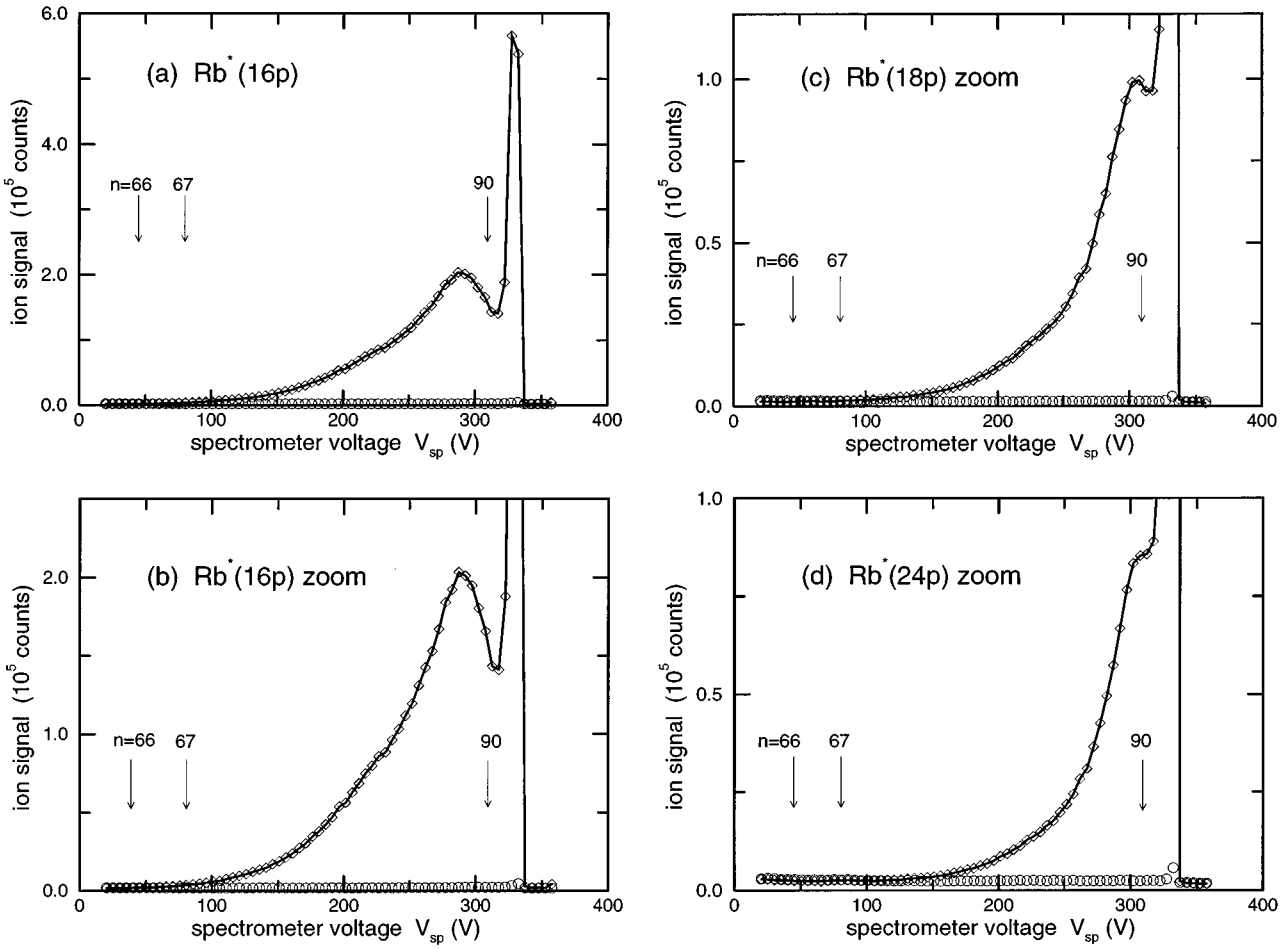

FIG. 4. Kr^{7+}* ion spectra for capture from Rb*($n_i p$) into Kr^{8+} at 18 keV, for $n_i p = 16p$ (a) and (b), $18p$ (c), and $24p$ (d); ◇ joined by a continuous line, laser on; ○ laser off. The Kr^{7+}* ions are detected as Kr^{8+} ions, on the channeltron, after field ionization in the FILS. The Kr^{8+} kinetic energy is related to the SP2 spectrometer voltage by $\simeq 54.4 \times V_{sp}$ (in eV).

three energy spectra of the product Kr^{8+} ions resulting from field ionization of the $Kr^{7+}(n)$ ions are shown in Fig. 4 for Rb*($16p$), Rb*($18p$), and Rb*($24p$).

Over the whole series, it is observed that the Kr^{8+} ion spectrum due to the field ionization of Kr^{7+}*(n) ions vanishes completely when the laser is blocked. It then reduces to a nearly negligible constant background of a few hundred counts (see Figs. 4–6). The great majority of Kr^{7+} ions cannot be field ionized. They are easily detected after the SP2 with the Faraday cup FC2 at the order of magnitude of nA's (see Fig. 3). The small fraction of field ionized Kr^{7+} ions are detected as Kr^{8+} after the SP2 by a channeltron EM in counting mode. The absence of any substantial Kr^{8+} signal when the laser is off demonstrates the high efficiency of our detection method by field ionization, which discriminates completely against Kr^{7+} ions which cannot be field ionized.

The Kr^{8+} ion energy spectra in Fig. 4 are composed only of the signal due to field ionization of the Rydberg $Kr^{7+}(n)$ ions. In these spectra, Kr^{8+} ions with increasing kinetic energy E_f' correspond to Kr^{7+}*(n) ions with increasing values of n. Rydberg levels in Kr^{7+}*(n) with high n are field ionized with a small F_j existing close to the FILS entrance, corresponding to a small $|U_j|$. From Eq. (5), one can deduce that these ions leave the FILS with a kinetic energy near its maximum value $E_f' = E_0$. Contrarily, Kr^{7+}*(n) ions in Rydberg levels with the lowest n, which are field ionized with the largest F_j existing close to the center z_c of the FILS, experience a large $|U_j|$. These ions leave the FILS with a minimum kinetic energy $E_f' = E_0 - e|U_m|$, where U_m is the potential at z_m where the field reaches its maximum F_m. $|U_m|$ is slightly smaller than the maximum value of the potential $|U_z|$. Consequently, all the n levels more tightly bound than that which is field ionized by F_m are not detected. This creates a lower limit to the detection window in the present experiment: $n \simeq 66$ for the second set of potentials which generates $F_m = 9.1$ kV/cm.

The narrow peak close to E_0 stems from very high Rydberg levels which are ionized near the small diaphragm at the entrance of the FILS (see Sec. II. A 4). The diaphragm produces over the first few millimeters of the lens an increase of the axial field sharper than the linear variation existing along most of the z axis of the FILS. Therefore a significant number of high n states is field ionized in a region of relatively small decrease of potential. All Rydberg levels with n above a certain value are field ionized in this region and show up within a very narrow band of kinetic energies E_f' For the second set of potentials that is used here, all the n values higher than 95 are packed up inside this peak. This peak is not an artifact; the ion signal simulated by using a realistic n-dependent analytical cross section produces an ion spec-

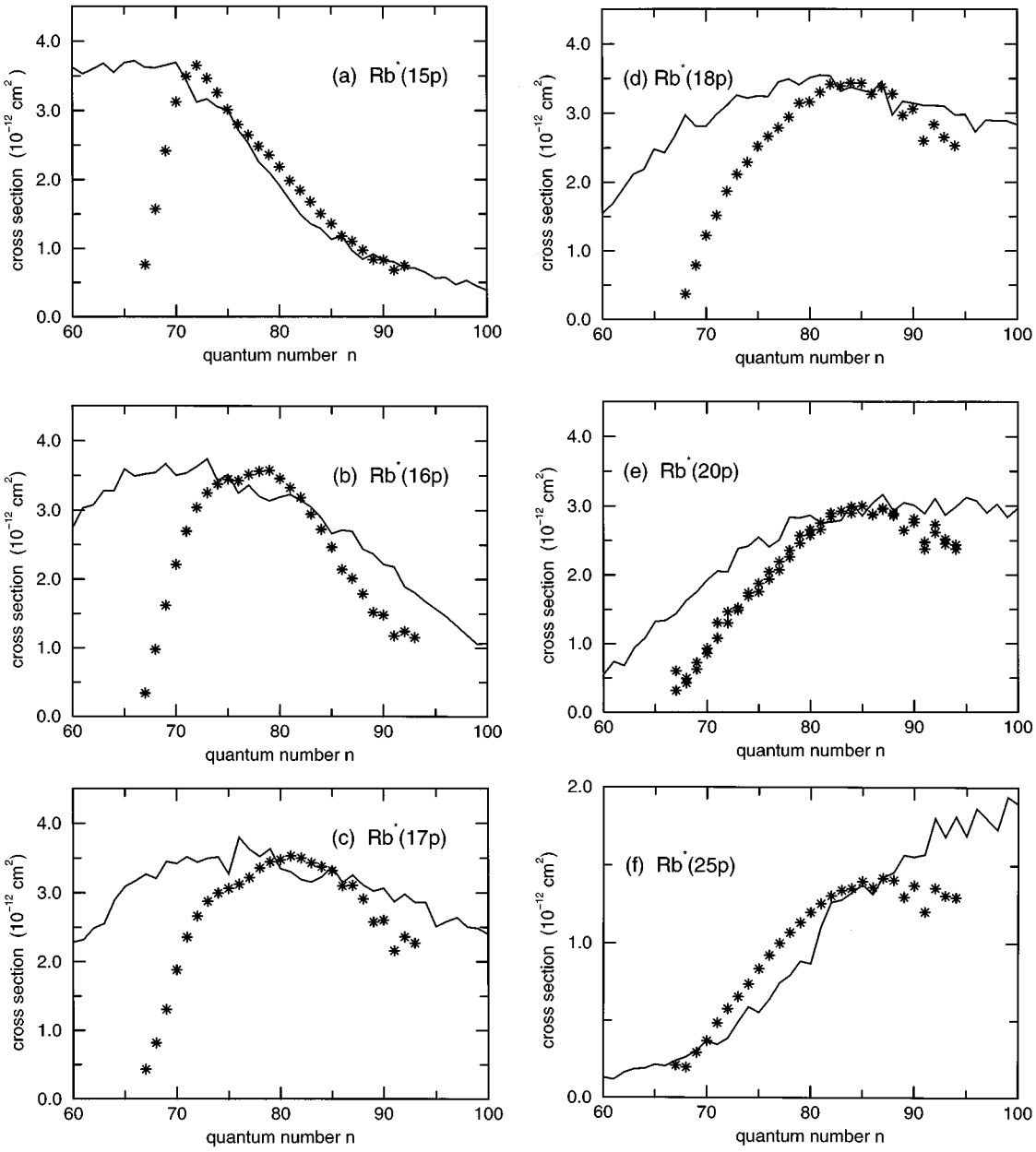

FIG. 5. Experimental cross section $\sigma_{\text{expt}}(n)$ for capture from Rb*$(n_i p)$ into Kr^{8+} at 18 keV, for $n_i p = 15p$ (a), $16p$ (b), $17p$ (c), $18p$ (d), $20p$ (e), and $25p$ (f), versus quantum number n defined within the classical field ionization model using $F_c(n) = q^3/(16n^4)$: *. The CTMC capture cross section $\sigma_{\text{theor}}(n)$ calculated for each value of n is represented by a continuous line. The cross section σ_{expt} has been normalized to the CTMC calculation.

trum with a behavior similar to the experimental one, including the narrow peak. This means that the signal included in this peak does belong to the physical process under consideration. However, the tightening of the Rydberg levels inside this peak — both because of the density of Rydberg states per energy interval increasing with n, and because of the potential geometry at the FILS entrance—is such that we limit the treatment of the signal to the detection window $67 \leqslant n \leqslant 95$ for $F_m = 9.1$ kV/cm.

The experimental design requires electric fields along the whole ion path, the presence of which is unavoidable. For instance, the excited ions with $n \geqslant 135$ are already ionized in the SP1, before the FILS, where the radial field is close to 500 V/cm for the present experimental conditions.

All the data show the same type of behavior, but we do observe systematic shifts in our ion spectra depending on the initial state of excitation of Rb*. As n_i in Rb* increases, the maximum close to the left of the narrow peak shifts towards higher V_{sp}. This is a logical behavior: it is explained by the decreasing binding energy ϵ_{at} of the excited electron in Rb* which results in the capture towards higher and higher Rydberg levels in Kr^{7+}*.

B. Experimental cross sections

The treatment of the data for the deduction of the experimental cross section $\sigma_{\text{expt}}(n)$ from the Kr^{8+} ion spectra follows several steps: (i) all the voltages are corrected in agree-

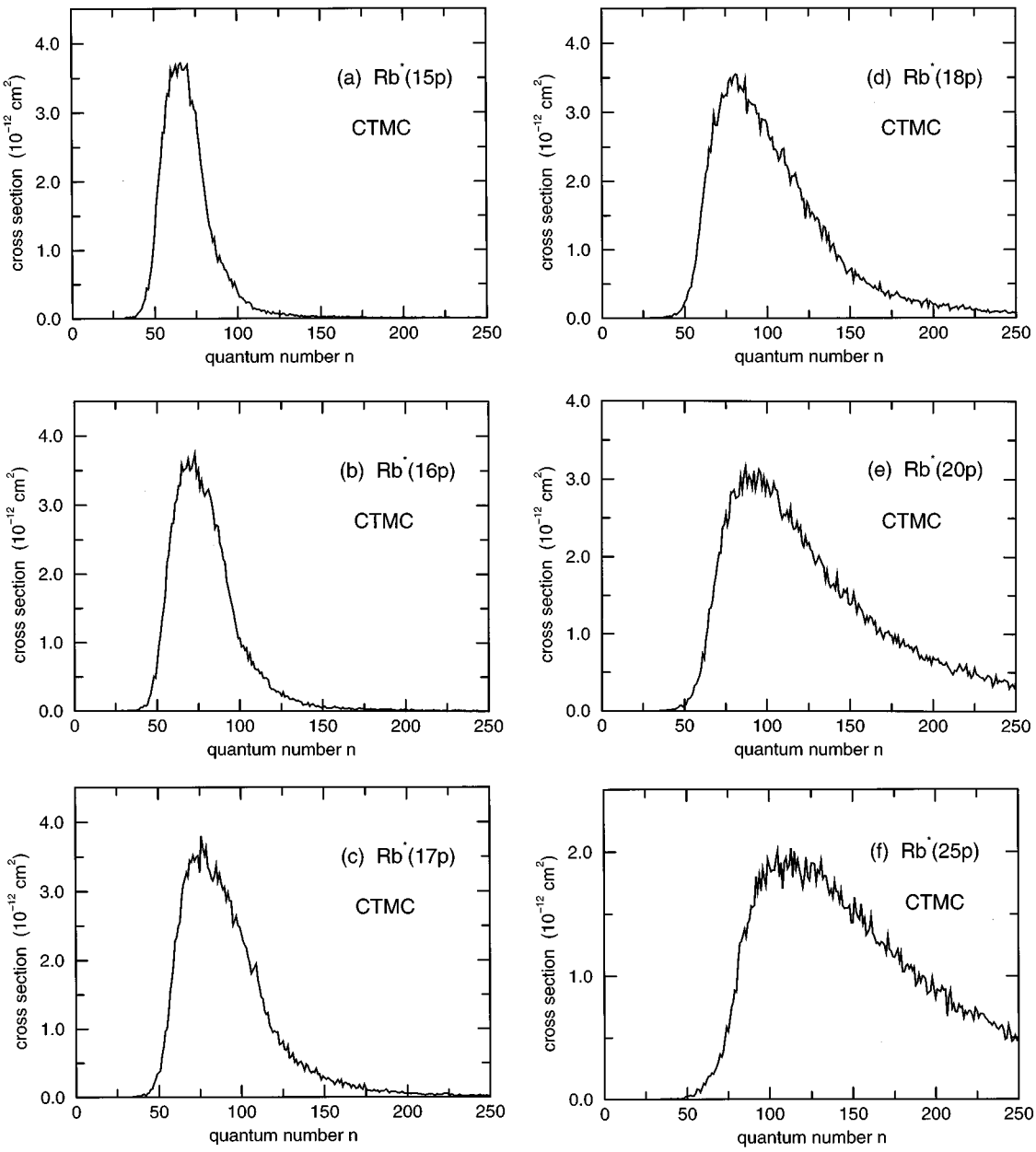

FIG. 6. CTMC theoretical cross section $\sigma_{\text{theor}}(n)$ for capture from Rb*$(n_i p)$ into Kr^{8+} at 18 keV, for $n_i p = 15p$ (a), $16p$ (b), $17p$ (c), $18p$ (d), $20p$ (e), and $25p$ (f), calculated for every value of n but represented by a continuous line as in Fig. 5.

ment with the calibration, and the positive plasma potential in the ion source is taken into account to define E_0 (E_0 = 18.17 keV); (ii) the background ion spectrum with the laser off is subtracted from the ion spectrum with the laser on; (iii) the constant resolution of the detection system $R = E_f'/\Delta E_f' = V_{\text{sp}}/\Delta V_{\text{sp}} \simeq 90$ (FWHM) causes the detection width ΔV_{sp} to increase linearly with V_{sp}. The number of counts in every channel of the spectra of the Kr^{8+} product ions after field ionization is divided by V_{sp} to compensate for this effect. This $1/E_f'$ correction has been verified to be sufficiently accurate.

The experimental cross section is obtained using the critical field of the classical field ionization model $F_c(n) = q^3/(16n^4)$. This hypothesis allows a direct mapping of the kinetic energy of the ion E_f' onto the field F_j in the FILS. For a given n_j value and the relevant classical field $F_c(n_j)$, the corresponding z_j distance and U_j potential in the FILS are deduced by using a high precision electrostatic lens analysis program [23]. The final kinetic energy E_f' is deduced by Eq. (5), and the relevant V_{sp} spectrometer voltage by the SP2 calibration parameter k.

The discrete character of the n levels, in contrast to the continuity of the V_{sp} voltage, is taken into account by attributing all the ion signal within the range $[F_c(n_j), F_c(n_j - 1)]$ to the n_j level. Consequently, $\sigma_{\text{expt}}(n_j)$ (in arbitrary units) is derived by integrating the ion signal over the interval $[V_{\text{sp}}(n_j - 1), V_{\text{sp}}(n_j)]$. This procedure is applied to the eleven spectra $15p \leqslant n_i p \leqslant 25p$. Six of them,

for $n_i p = 15p-18p$, $20p$, and $25p$, are shown in Fig. 5.

For the highest Rb excited states $n_i p \geqslant 20p$, the difference between the various $\sigma_{\text{expt}}(n)$ becomes tenuous, though visible. This is mainly due to the tightening of the excited states of Rb. In the hydrogenic approximation, the gap $\delta\epsilon_{\text{at}}$ between two adjacent levels decreases as n^{-3}; using the precise values for Rb, this effect can be illustrated by the gap between the $21p$ and $25p$ states which is equal to that between the $15p$ and $16p$ states.

For all the Rb* states, very high Rydberg levels are detected. They are distributed on wide and bell-shaped distributions, centered on $n = 75-88$ depending on the Rb initial state between $15p$ and $25p$. Since all the measurements for this series have been made with the highest set of voltages on the FILS, corresponding to $F_m = 9.1$ kV/cm, the detection window covers the domain 67–95. In our previous work [4], the cross section $\sigma_{\text{expt}}(n)$ for Kr^{8+} + Rb*$(17p)$ at 40 keV has been presented in the domain 67–110. This is the result of bringing together two measurements of the same process using the two sets of voltages on the FILS; the lowest giving information in the domain 75–110, and the highest in the domain 67–95.

We do observe a systematic evolution of the shape of the $\sigma_{\text{expt}}(n)$ cross sections. A broadening, together with a slight displacement of the maximum towards high n, is clearly shown when the initial state of Rb is scanned unit by unit from $15p$ to $25p$. For Rb*$(15p)$, $\sigma_{\text{expt}}(n)$ exhibits a sharp maximum at $n \simeq 72$ and a width (FWHM) $\Delta n \simeq 14$. For Rb*$(16p)$, $\sigma_{\text{expt}}(n)$ exhibits a less sharp maximum at $n \simeq 77$ and a width $\Delta n \simeq 19$. For Rb*$(17p)$, $\sigma_{\text{expt}}(n)$ exhibits a flatter maximum at $n \simeq 81$ and its width [which is obtained via a slight extrapolation of $\sigma_{\text{expt}}(n)$ towards the high n] is $\Delta n \simeq 25$. For the still higher Rb* levels, the width (FWHM) cannot be deduced any longer because the cross section at the higher threshold of the detection window does not drop to HM. But the behavior of $\sigma_{\text{expt}}(n)$ around the maximum tends to become flatter and flatter, indicating a broadening of the n distribution. For Rb* in the states $(18p)$, $(19p)$, and above, the maxima are located at $n \simeq 84$, 86, and tend to stabilize at $\simeq 88-90$ for $n_i p \geqslant 20p$.

IV. THEORETICAL CALCULATIONS

The collision between the ion Kr^{8+} and the target atom Rb*$(n_i p)$ is reduced to a three-body collision problem: the two ionic cores Kr^{8+} and Rb^{+}, and the excited valence electron e. Since the two cores have closed shells, a local model potential is well adapted to describe the effective interaction between the active electron and each of the two cores. We have used

$$V_{\text{Rb}^+}(r) = -\frac{1}{r}(1 + 36e^{-3.333r} + 6.429re^{-1.369r}) \qquad (6)$$

for the e-Rb^{+} interaction [24], and

$$V_{\text{Kr}^{8+}}(r) = -\frac{1}{r}(8 + 28e^{-4.75r} + 5.7re^{-3.52r}) \qquad (7)$$

for the e-Kr^{8+} interaction [16]. The parameters of the potentials have been determined to fit spectroscopic data. The potentials have the correct behavior at large and small distances r.

The three-body CTMC method is based on solving Hamilton's equations for the three classical particles (the two cores and the active valence electron), given the initial conditions for the target and the projectile. As in previous calculations [15,16], the method used for sampling the initial state of Rb* from a microcanonical distribution is that of Ref. [25]. The binning procedure of the classical quantities (energy, angular momentum vector of the electron, and its projection along the initial velocity direction of the projectile taken as quantization axis) to determine the final n,l,m distributions of the captured electron has been developed previously [26,27]. Let us note that the asymptotic quantum defects $\delta(l)$ of the Kr^{7+}* ion are considered in the procedure, although the core-electron effect of the projectile, which populates significantly low values of l in the capture from a ground-state target [16], is much less important in the capture from Rydberg-state Rb* atoms. In the latter case, large l values are predominantly produced (see Sec. V B).

Our CTMC n distributions are calculated with a sufficient number of classical trajectories (between 1.5×10^5 and 5×10^5) to provide statistical uncertainties less than 5% near the maximum and less than 10% in the edges. The $\sigma_{\text{theor}}(n)$ distributions at 18 keV, for $n_i p = 15p$ to $18p$, $20p$, and $25p$ shown in Fig. 6, extends over larger and larger domains as $n_i p$ increases. While the lower limit of the domains varies over the small interval $n \simeq 40$ to 50 as $n_i p$ increases from $15p$ to $25p$, the higher limit varies over the wide interval $n \simeq 110$ to more than 250 [the limits defined here are such that $\sigma_{\text{theor}}(n)$ exceeds $0.05 \times \sigma_{\text{theor}}^{\max}$]. The maxima are distributed from $n \simeq 65$ to 93 for $n_i p$ varying from $15p$ to $20p$, and pushed to $n \simeq 110$ for $n_i p = 25p$; their amplitude $\sigma_{\text{theor}}^{\max}$ decreases slowly from $\simeq 3.7\times10^{-12}$ cm^2 to $\simeq 2\times10^{-12}$ cm^2. However, since the width of the distributions increases substantially as $n_i p$ increases, the total capture cross section increases significantly (from $\simeq 1.2\times10^{-10}$ cm^2 to $\simeq 2.3\times10^{-10}$ cm^2 for $n_i p$ varying from $15p$ to $25p$), but not as much as would be expected from simple considerations of the geometric cross sections. This can be explained by the increasing weight of the ionization channel when $n_i p$ increases, compared to that of electron capture; the ratio of the total cross sections for the electron capture and the ionization $\sigma_{t,\text{theor}}/\sigma_{t,\text{theor}}^{+}$ varies from 77 to 0.5 between $15p$ and $25p$. This originates in the increase of the reduced velocity $\tilde{v} = v_p/v_e$ from 1.14 to 2.07 between $15p$ and $25p$ for the projectile energy of 18 keV. For Rb*$(25p)$, the large cross section for ionization may explain the large extent of the n distribution of the capture cross section σ_{theor} towards very high n (as possible channels to ionization).

V. DISCUSSION AND CONCLUSION

A. Comparison of experimental results with theoretical calculations

Comparison of the experimental cross sections with the theoretical CTMC ones shows a reasonable agreement as far

as the overall behaviors (i) of the cross section with n (for a given $n_i p$), and (ii) of the n distribution of the cross section with $n_i p$, are concerned. We observe that the maximum of the CTMC $\sigma_{\text{theor}}(n)$ is shifted in the same direction as that of the experimental $\sigma_{\text{expt}}(n)$ when $n_i p$ varies from $15p$ to $25p$, but by a larger amount, however. The maxima of the 11 $\sigma_{\text{theor}}(n)$ of the series $15p$–$25p$ are spread over an interval $n \simeq 64$ to $n \simeq 105$, which is larger than that observed for the $\sigma_{\text{expt}}(n)$ given by $n \simeq 72$ to $n \simeq 90$. The width of $\sigma_{\text{theor}}(n)$ increases when $n_i p$ varies from $15p$ to $25p$ as does that of $\sigma_{\text{expt}}(n)$; it remains, however, always larger. For the cases where the whole width FWHM is measured, we observe that $\sigma_{\text{theor}}(n)$ has a width larger than $\sigma_{\text{expt}}(n)$ by a factor of $\simeq 2$.

In the classical over-the-barrier (CB) model, scaling laws indicate that the capture of an electron of binding energy ϵ_{at} in Rb* proceeds with a quasiconservation of this binding energy. The binding energy ϵ_{ion} of the captured electron in the $Kr^{(q-1)+}$* ion is given by

$$\epsilon_{\text{ion}} = \epsilon_{\text{at}} / g^2(q), \tag{8}$$

where the function $g^2(q)$ is given by

$$g^2(q) = (1 + 2\sqrt{q})/(q + 2\sqrt{q}). \tag{9}$$

$g(q)$ slightly decreases from 1 to 0.7 for q varying from 1 to 8. If we adopt the hydrogenic approximation for the excited levels in both the excited Rb* atom and Kr^{7+}* ion, Eq. (8) reduces to

$$n = q g(q) n_i . \tag{10}$$

Within this framework, a unique n state is populated in the capture process, the value of which increases from $n = 84$ to 140 by steps of five or six, for $n_i p$ increasing from $15p$ to $25p$ by steps of one. We observe that the range of variation of this unique level n is larger than that of the maximum of both the experimental and CTMC n distributions and is shifted towards higher n.

In comparison, the extended classical over-the-barrier (ECB) model [3] yields n distributions with positions of maxima increasing from $n = 69$ to 125. We have calculated these distributions and normalized them according to

$$\sigma(n) = \pi R_c^2 n^2 W(\epsilon) / \sum_k n_k^2 W(\epsilon_k), \tag{11}$$

where R_c is the capture radius and $W(\epsilon_k)$ is the reaction window in the space of binding energies of the captured electron in the product ion ϵ, as defined in Ref. [3]. Summation is made over all the n_k levels populated in the Kr^{7+}* ion. The agreement with the experimental distributions is satisfactory as far as the positions of maxima for the $15p$–$18p$ states are concerned; for higher states, the ECB maxima are at higher n values. Four of the resulting ECB distributions are shown in Fig. 7. The ECB model is not basically kinetic-energy dependent, although it includes some dynamical features. The width of the ECB distributions arises from uncertainty in the height of the potential barrier due to limited transition time. A comparison of the ECB distributions with either the experimental ones or the CTMC ones at 18 keV shows that they are narrower than the experimental ones by a factor of $\simeq 2$ (for the $15p$) to 3 (for the $17p$ and higher states), and narrower than the CTMC ones by a factor of $\simeq 4$ to 6.

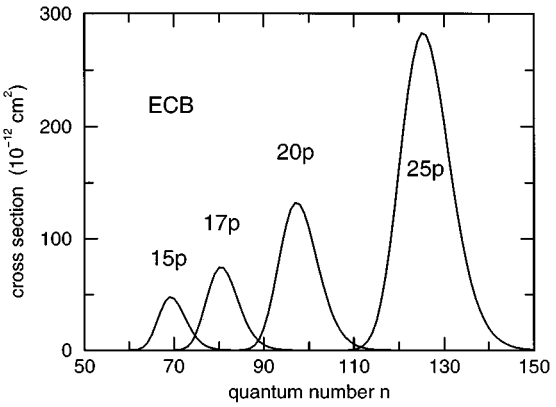

FIG. 7. ECB theoretical cross sections calculated as defined in the text (see Sec. V A) for capture from Rb*($n_i p$) into Kr^{8+} at 18 keV, for $n_i p = 15p$, $17p$, $20p$, and $25p$.

From Ref. [28], the ECB model should be valid only for $\tilde{v} = v_p / v_e \ll 1$. In the present experiment, $\tilde{v}$ varies from 1.14 to 1.61 in the interval $15p$–$20p$ and reaches 2.07 for the $25p$. Therefore its application is just indicative. A Rydberg-state target atom has a very slow peripheral electron: $v_e = 0.081$ a.u. for the $15p$ orbital and $v_e = 0.044$ a.u. for the $25p$ orbital. The production of a sufficiently intense beam of eight-times charged ions is facilitated by a relatively high kinetic energy of the projectile. Approaching collisional conditions close to the matching velocity $\tilde{v} \simeq 1$ is already difficult in the present experiment. Obtaining $\tilde{v} \ll 1$ would have required an improved ion optics at the entrance and exit of the target box.

B. Approximations in the determination of the experimental cross sections

The n distributions derived from our experimental data rely on several approximations.

The first point concerns the use of the classical model for field ionization. In this model, the ionization probability of a Rydberg n state equals one as soon as the electric field exceeds the classical field $F_c(n) = q^3/(16n^4)$, and zero if it does not. In this framework, only the height of the potential barrier between the electron and the core in the presence of an electric field is considered; this effect is n-dependent only.

In the quantum mechanical treatment, the electron may escape from the atom by tunneling through the barrier, which depends on the probability of presence of the electron close to the barrier. Every n state separates into Stark substates which ionize with different probabilities, resulting in the emergence of adiabatic and diabatic SFI (state-selective field-ionization) peaks. Quantum mechanical calculations of the F-dependent ionization probability $\Gamma(F, n_+, n_-, m)$, as a

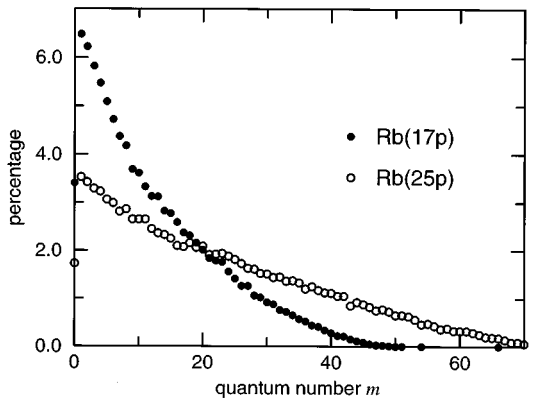

FIG. 8. Distributions of m sublevels of the total cross section $\sigma_{t,\mathrm{theor}}$, calculated by the CTMC method, for capture from Rb*$(17p)$ and Rb*$(25p)$ into Kr^{8+} at 18 keV.

function of the parabolic quantum numbers n_+, n_-, m (for all l values from 0 to $n-1$), for Rydberg states of hydrogen which ionize diabatically, actually show very strong variations with the field strength. For instance, for the two extreme $m=0$ Stark substates of $n=10$ ($n_+ = 9$, $n_- = 0$ and $n_+ = 0$, $n_- = 9$), Γ increases by factors of 3×10^6 and 2×10^7, respectively, for a field increase of about 50% [29]. Furthermore, the field values leading to neighboring values of Γ are different (by a factor of nearly 2), depending on whether the upper or the lower extreme substate is considered. As a consequence, the diabatic SFI signals are expected to be dependent on the experimental conditions of observation period and field slew rate; they have been generally observed for field values larger than the classical field $F_c(n)=q^3/(16n^4)$ in the case of laser excitation of specific high n, low l, and m states [30,31].

In the present case, very high Rydberg n states close to 100 are populated, with certainly wide but not experimentally accessible m distributions. However, our CTMC calculations predict these distributions for the total capture process $\sigma_{t,\mathrm{theor}}$ (see Fig. 8). At 18 keV, and for $n_i p = 15p$, $17p$, $20p$, and $25p$, for instance, the m distributions (with summation over n and l) are all peaked at $m=1$, but are quite broad. It is expected that states with $m = 0$, 1, and perhaps 2 ionize mainly adiabatically while those with $m \gtrsim 3$ mainly diabatically. The exact determination of the field ionization probabilities for all Stark substates with the present n,l,m distributions would require an enormous amount of work not possible at the present time. In such a context, the classical field ionization model, albeit not exact since it ignores tunneling ionization, can be revisited, especially after the series of works devoted to SFI (see, for instance, [32]), which demonstrates that this model is physically justified and that the notion of a discontinuous threshold is reasonable. However, field values responsible for adiabatic and diabatic ionization appear to be included in the range $F_c(n)=q^3/(16n^4)$ to $q^3/(9n^4)$, rather than defined by its lowest limit.

To illustrate the effect of such a higher ionizing field on the determination of the n distributions, a second treatment of the data with $F_c(n)=q^3/(9n^4)$ is made. We observe that the effect consists of a moderate shift towards higher n and a slight broadening of the experimental n distributions: the

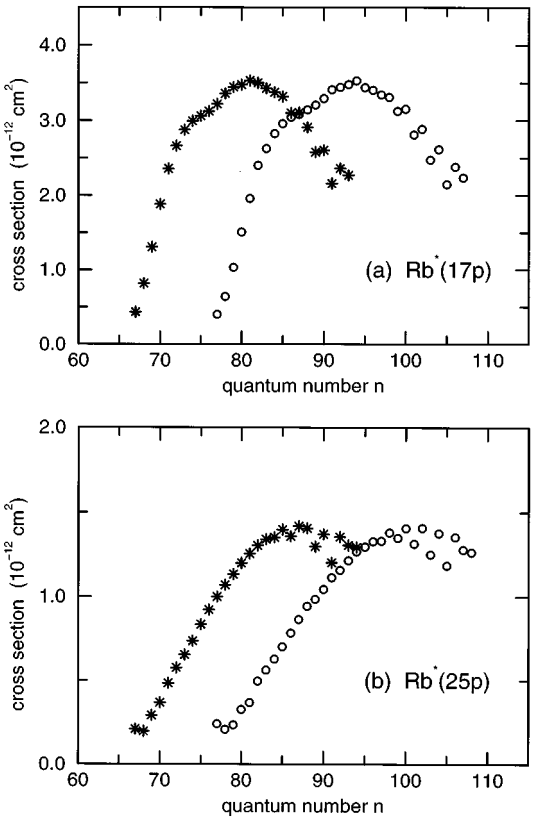

FIG. 9. Experimental cross section $\sigma_{\mathrm{expt}}(n)$ for capture from Rb*$(17p)$ (a), and Rb*$(25p)$ (b), into Kr^{8+} at 18 keV, versus quantum number n; *, obtained with $F_c(n)=q^3/(16n^4)$; ○, obtained with $F_c(n)=q^3/(9n^4)$.

shift by δn of the maximum of the distribution varies from $\delta n \simeq 11$ to $\simeq 14$ when scanning the series $15p$–$25p$, and the width is no more than 15% larger (for any Rb* state). Examples are given in Fig. 9. We observe, finally, that the shape of the $\sigma_{\mathrm{expt}}(n)$ distributions is not much affected by the choice of the function $F_c(n)$, but that their positions are moderately sensitive to it. We can consider that the two n distributions issued from $q^3/(16n^4)$ and $q^3/(9n^4)$ delimit a region where the exact distribution is located. One can conclude that using the classical field ionization model gives a reasonable estimate of the positions and shapes of the n distributions.

The second point concerns the lifetime of the excited $Kr^{7+}*(n)$ ions. At 18 keV, the transit time between the target region where these ions are created and the FILS is about 2 μs. The lifetime of such ions is not available in the literature, but it can be estimated, in a first approximation, by the scaling law

$$\tau(n)=\tau_0(n_0)\left(\frac{n}{n_0}\right)^{4.5}\left(\frac{q_0}{q}\right)^4. \qquad (12)$$

In this formula, the lifetime is averaged over statistical populations of l sublevels (all l values from 0 to $n-1$). With a hydrogenic lifetime for the reference value $\tau_0(n_0)$, for instance, that of H*$(n_0=6)$ equal to 0.196 μs [33], one obtains $\tau(n)$ distributed between 2.5 μs for $n = 67$, and 15 μs for $n = 100$. This suggests that a fraction of the excited

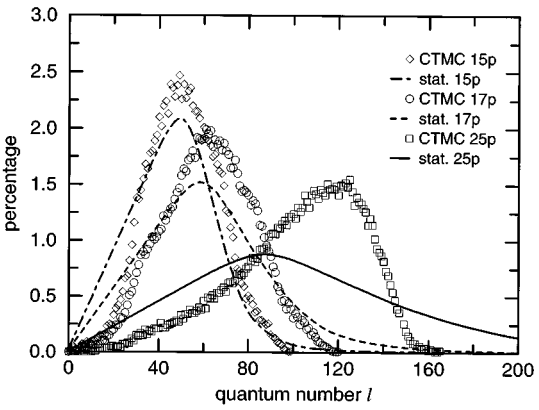

FIG. 10. Distributions of l sublevels of the total cpture cross section $\sigma_{t,\mathrm{theor}}$; $\diamond$, $\circ$, $\square$, calculated by the CTMC method (with summation on CTMC n and m distributions); dot-dashed, dashed, solid lines, calculated within the hypothesis of a statistical population of l sublevels weighted by the CTMC n distribution (with summation on CTMC n distributions and on statistical m distributions). Capture from Rb*$(15p)$, Rb*$(17p)$, and Rb*$(25p)$ into Kr^{8+} at 18 keV.

Kr^{7+}*(n) ions with the lowest n levels would not reach the FILS, and consequently that the related ionic signal could be underestimated owing to the short lifetimes.

Electron capture, however, is not expected to produce a statistical population of l sublevels. These populations are not accessible in the present experiment but can be approximated by the CTMC ones. The l-specific lifetimes can be estimated by the scaling law

$$\tau(n,l)=\tau_0(n_0,l)\left(\frac{n}{n_0}\right)^3\left(\frac{q_0}{q}\right)^4. \tag{13}$$

By using the hydrogenic lifetimes up to $l=12$ of Ref. [34] for the reference value $\tau_0(n_0,l)$, one can estimate directly all the $\tau(n,l)$ for $l \leqslant 12$, and, after an extrapolation, all the $\tau(n,l)$ for $l \geqslant 12$. For 18 keV, the CTMC l distribution of the total capture cross section $\sigma_{t,\mathrm{theor}}$ is calculated; it is compared with the l distribution calculated with a statistical population of l sublevels weighted by the present CTMC n distribution for Rb*$(15p)$, Rb*$(17p)$, and Rb*$(25p)$, in Fig. 10.

In the case of Rb*$(17p)$, one observes that the population of the lowest l sublevels, $l \leqslant 15$, is negligible, which causes the lifetimes to be always larger than 1.6 μs, a time which is comparable to the transit time [the shortest lifetimes being those of the $n=67$ state, the shortest l-specific lifetime is $\tau(67,15) \simeq 1.6$ μs]. One observes also that the sublevels with $l \leqslant 45$ are still under-represented compared to the statistical distribution; the shortest related lifetime is $\tau(67,45) \simeq 14$ μs. This means that τ ($n=67$, averaged over all l) is obviously $\gg 14$ μs, particularly when one observes that the l distribution has its maximum at $l = 60$ which corresponds to a lifetime $\tau(67,60) \simeq 24$ μs. Since all the lifetimes $\tau(n \geqslant 67, l \geqslant 60)$ are still longer, we neglect the effect of the transit time from the target to the ionizing lens.

In the case of Rb*$(25p)$, one observes that much higher l sublevels are populated, yielding much longer lifetimes. The sublevels with $l \leqslant 27$ are not populated, which indicates that the l-specific lifetimes are always larger than 4.5 μs, a time already longer than the transit time. The sublevels with $l \leqslant 80$ are still under-represented; the shortest related lifetimes are $\tau(67,66) \simeq 29$ μs and $\tau(81,80) \simeq 72$ μs, which largely exceed the transit time. Therefore, for this state, we can conclude that no loss of ions may happen, especially when noting that the l distribution has its maximum at extremely high l ($l = 120$).

In the case of Rb*$(15p)$, one observes that the domain where the l sublevels are under-represented extends to $l \simeq 33$; the shortest related lifetime is $\tau(67,33) \simeq 7.6$ μs. This value [to be compared with 14 μs in the case of Rb*$(17p)$] does not exceed largely the transit time, involving a possible loss of ions. This feature could explain the specific shape of $\sigma_{\mathrm{expt}}(n)$, which decreases more deeply than all the others when n decreases under 72.

C. Conclusion

We have observed very high Rydberg levels in Kr^{7+}*(n) ions produced after single electron capture from a series of Rb*(n_ip) Rydberg atoms, excited separately by a monochromatic laser light at about 300 nm. For every well-defined Rb*(n_ip) state, a wide n distribution of the capture cross section has been obtained, extending up to very high n levels close to 100. We do observe a systematic evolution of the shape of the $\sigma_{\mathrm{expt}}(n)$ cross sections: a broadening, together with a slight displacement of the maximum towards high n is clearly shown when the initial state of Rb is scanned unit by unit from $15p$ to $25p$.

The comparison with our theoretical results based on CTMC calculations shows a reasonable agreement as far as the overall behaviors of the cross section with n (for a given n_ip), and of the n distribution of the cross section with n_ip, are concerned. When n_ip varies from $15p$ to $25p$, we observe (i) that the maximum of the CTMC $\sigma_{\mathrm{theor}}(n)$ cross section is shifted in the same way as that of the experimental $\sigma_{\mathrm{expt}}(n)$ cross section, by a larger amount, however, and (ii) that the width of the CTMC $\sigma_{\mathrm{theor}}(n)$ increases as does that of $\sigma_{\mathrm{expt}}(n)$, while remaining, however, always larger [by a factor of about 2 for the cases where the whole width (FWHM) is measured].

The n distributions of $\sigma_{\mathrm{expt}}(n)$ are observed to be broader than those predicted by the ECB model, which yields widths about two to three times smaller, for this kinetic energy. This is a confirmation of the ability of the ECB model to explain capture on atoms in the ground state or in the first resonant state only, where the velocity of the electron to be captured is much larger than that of the projectile. This is not the case for our target atoms in Rydberg states.

ACKNOWLEDGMENTS

We would like to thank A. Brenac, G. Lamboley, and T. Lamy for providing intense and stable multicharged ion beams. We are also grateful to F. B. Dunning, T. F. Gallagher, E. Luc-Koenig, K. B. MacAdam, R. E. Olson, and C. O. Reinhold for fruitful discussions. The AIM/ex-LAGRIPPA is a joint facility of the Commissariat à l'Energie Atomique (CEA) and of the Centre National de la Recherche Scientifique (CNRS).

[1] R. E. Ryufuku, K. Sasaki, and T. Watanabe, Phys. Rev. A **21**, 745 (1980).
[2] A. Bárány, G. Astner, H. Cederquist, H. Danared, S. Huldt, P. Hvelplund, A. Johnson, H. Knudsen, L. Liljeby, and K. G. Rensfelt, Nucl. Instrum. Methods B **9**, 397 (1985).
[3] A. Niehaus, J. Phys. B **19**, 2925 (1986).
[4] A. Pesnelle, R. Trainham, J. Pascale, E. Monnand, and H. J. Andrä, Phys. Rev. Lett. **74**, 4169 (1995).
[5] R. G. Rolfes and K. B. MacAdam, Phys. Rev. A **15**, 4591 (1982).
[6] K. B. MacAdam, L. G. Gray, and R. G. Rolfes, Phys. Rev. A **42**, 5269 (1990).
[7] K. B. MacAdam, in *Electronics and Atomic Collisions*, edited by T. Andersen, B. Fastrup, F. Folkmann, H. Knudsen, and N. Andersen (AIP Press, New York, 1993), p. 183, and references therein.
[8] F. Aumayr, M. Gieler, E. Unterreiter, and H. Winter, Europhys. Lett. **16**, 558 (1991).
[9] F. Aumayr, M. Gieler, J. Schweinzer, H. Winter, and J. P. Hansen, Phys. Rev. Lett. **68**, 3277 (1992).
[10] M. Gieler, F. Aumayr, J. Schweinzer, W. Koppensteimer, W. Husinsky, H. P. Winter, K. Lozhkin, and J. P. Hansen, J. Phys. B **26**, 2137 (1993).
[11] A. R. Schlatmann, R. Hoekstra, R. Morgenstern, R. E. Olson, and J. Pascale, Phys. Rev. Lett. **71**, 513 (1993).
[12] S. Schippers, A. R. Schlatmann, W. P. Wiersema, R. Hoekstra, R. Morgenstern, R. E. Olson, and J. Pascale, Phys. Rev. Lett. **72**, 1628 (1994).
[13] B. D. DePaola, M. T. Huang, S. Winecki, M. P. Stöckli, Y. Kanai, S. R. Lundeen, C. W. Fehrenbach, and S. A. Arko, Phys. Rev. A **52**, 2136 (1995).
[14] R. E. Olson, J. Phys. B **13**, 843 (1980).
[15] J. Pascale, R. E. Olson, and C. O. Reinhold, Phys. Rev. A **42**, 5305 (1990).
[16] E. Jacquet, P. Boduch, M. Chantepie, M. Druetta, D. Hennecart, X. Husson, D. Lecler, F. Martin-Brunetière, R.E. Olson, J. Pascale, and M. Wilson, Phys. Scr. **49**, 154 (1994).
[17] T. Lamy, G. Lamboley, D. Hitz, and H. J. Andrä, Rev. Sci. Instrum. **61**, 336 (1990).
[18] A. Pesnelle, M. Perdrix, and G. Watel, Opt. Commun. **96**, 4303 (1992).
[19] S. Runge, A. Pesnelle, M. Perdrix, D. Sevin, N. Wolffer, and G. Watel, Opt. Commun. **42**, 45 (1982).
[20] F. Gounand, J. Phys. (Paris) **40**, 457 (1979).
[21] R. Trainham, A. Pesnelle, E. Monnand, M. Benhenni, and H. J. Andrä (unpublished).
[22] A. Pesnelle and H. J. Andrä (unpublished).
[23] In a first step, the SIMION electrostatic lens analysis program in its PC/PS2 version developed at the Idaho National Engineering Laboratory has been used to model the FILS. In a second step and the present work, a more flexible electrostatic lens analysis program developed by one of us (H.J.A.), with an increased resolution compared to SIMION, has been used.
[24] M. Klapisch, C. R. Acad. Sci. Ser. B **265**, 914 (1967).
[25] C. O. Reinhold and C. A. Falcon, Phys. Rev. A **33**, 3859 (1986).
[26] E. Jacquet, J. Pascale, P. Boduch, M. Chantepie, and D. Lecler, J. Phys. B **28**, 2221 (1995).
[27] C. Laulhé, E. Jacquet, G. Cremer, J. Pascale, P. Boduch, G. Rieger, D. Lecler, M. Chantepie, and J. L. Cojan, Phys. Rev. A **52**, 3803 (1995).
[28] A. Niehaus, Nucl. Instrum. Methods B **23**, 17 (1987).
[29] R. J. Damburg and V. V. Kolosov, in *Rydberg States of Atoms and Molecules*, edited by R. F. Stebbings and F. B. Dunning (Cambridge University Press, Cambridge, England, 1983), p. 31.
[30] T. F. Gallagher, L. M. Humphrey, W. E. Cooke, R. M. Hill, and S. A. Edelstein, Phys. Rev. A **16**, 1098 (1977); W. E. Cooke and T. F. Gallagher, *ibid.* **17**, 1226 (1978).
[31] T. J. Jeys, G. W. Foltz, K. A. Smith, E. J. Beiting, F. G. Kellert, F. B. Dunning, and R. F. Stebbings, Phys. Rev. Lett. **44**, 390 (1980); F. B. Dunning and R. F. Stebbings, in *Rydberg States of Atoms and Molecules*, edited by R. F. Stebbings and F. B. Dunning (Cambridge University Press, Cambridge, England, 1983), p. 315.
[32] P. Pillet, H. B. van Linden van den Heuvell, W. W. Smith, R. Kachru, N. H. Tran, and T. F. Gallagher, Phys. Rev. A **30**, 280 (1984).
[33] H. A. Bethe and E. E. Salpeter, *Quantum Mechanics of One- and Two-Electron Atoms* (Plenum Publishing Corporation, New York, 1977), p. 266.
[34] A. Lindgard and S. E. Nielsen, At. Data Nucl. Data Tables **19**, 633 (1977).